Earth and Planetary Science Letters 488 (2018) 144–154

Contents lists available at ScienceDirect

Earth and Planetary Science Letters

www.elsevier.com/locate/epsl

Length-scales of chemical and isotopic heterogeneity in the mantle section of the Shetland Ophiolite Complex, Scotland

B. O'Driscoll [a,*], R.J. Walker [b], P.L. Clay [a], J.M.D. Day [c], R.D. Ash [b], J.S. Daly [d,e]

[a] School of Earth and Environmental Sciences, University of Manchester, Manchester, UK
[b] Department of Geology, University of Maryland, College Park, MD, USA
[c] Scripps Institution of Oceanography, University of California San Diego, La Jolla, CA, USA
[d] UCD School of Earth Sciences and UCD Earth Institute, University College Dublin, Dublin, Ireland
[e] Irish Centre for Research in Applied Geosciences (iCRAG), Belfield, Dublin 4, Ireland

ARTICLE INFO

Article history:
Received 29 October 2017
Received in revised form 7 February 2018
Accepted 12 February 2018
Available online xxxx
Editor: F. Moynier

Keywords:
Shetland Ophiolite Complex
oceanic mantle
highly siderophile elements
Re–Os isotopes
mantle heterogeneity

ABSTRACT

Kilometre to sub-metre scale heterogeneities have been inferred in the oceanic mantle based on sampling of both ophiolites and abyssal peridotites. The ~492 Ma Shetland Ophiolite Complex (SOC) contains a well-preserved mantle section that is dominated by harzburgite (~70 vol.%) previously reported to have variable major and trace element compositions, yet dominantly chondritic initial $^{187}Os/^{188}Os$ compositions. To assess the preservation of compositional heterogeneities at sub-metre length-scales in the oceanic mantle, a ~45 m^2 area of the SOC mantle section was mapped and sampled in detail. Harzburgites, dunites and a pyroxenite from this area were analysed for lithophile and highly-siderophile element (HSE) abundances, as well as for $^{187}Os/^{188}Os$ ratios. Lithophile element data for most rocks are characteristic of supra-subduction zone (SSZ) metasomatic processes. Two dunites have moderately fractionated HSE patterns and suprachondritic $\gamma Os_{(492\ Ma)}$ values (+5.1 and +7.5) that are also typical of ophiolitic dunites generated by SSZ melt–rock interactions. By contrast, six harzburgites and four dunites have approximately chondritic-relative abundances of Os, Ir and Ru, and $\gamma Os_{(492\ Ma)}$ values ranging only from −0.6 to +2.7; characteristics that imply no significant influence during SSZ processes. Two harzburgites are also characterised by significantly less radiogenic $\gamma Os_{(492\ Ma)}$ values (−3.5 and −4), and yield Mesoproterozoic time of Re depletion (T_{RD}) model ages. The range of Os isotope compositions in the studied area is comparable to the range reported for a suite of samples representative of the entire SOC mantle section, and approaches the total isotopic variation of the oceanic mantle, as observed in abyssal peridotites. Mechanisms by which this heterogeneity can be formed and preserved involve inefficient and temporally distinct melt extraction events and strong localised channelling of these melts.

1. Introduction

Earth's mantle is structurally and compositionally heterogeneous at length-scales ranging from ocean basins to hand specimens of mantle peridotite. Understanding the timing and causes of these heterogeneities is important, given that mantle peridotites are key samples for defining the composition of the primitive mantle (PM) and for examining the timing and nature of planetary accretion and primary differentiation, as well as the evolution of plate tectonics (cf., Morgan, 1986; Morgan et al., 2001; Becker et al., 2006; Stracke et al., 2011; Rampone and Hofmann, 2012). Although studies have shown that some mantle domains may have survived the period of early-Earth differentiation to the present (Mukhopadhyay, 2012; Mundl et al., 2017), an array of processes have worked to destroy early-formed heterogeneities in upper mantle materials, such as convective mixing. New heterogeneities have also been created during partial melting and melt extraction, and lithospheric recycling and mantle metasomatism. These latter processes have led to the development of cm-to-km scale heterogeneities in the upper oceanic mantle (also termed depleted MORB mantle, or DMM; Dick et al., 1984; Snow et al., 1994; Workman and Hart, 2005; Liu et al., 2009; Warren et al., 2009). Compositional and isotopic heterogeneities reported from studies of oceanic mantle materials include refractory domains that are older than the presumed age of the mantle they are found in, and fertile components that may sample recycled crustal materials or 'frozen' upper mantle melt channels

* Corresponding author.
E-mail address: brian.odriscoll@manchester.ac.uk (B. O'Driscoll).

https://doi.org/10.1016/j.epsl.2018.02.020
0012-821X/

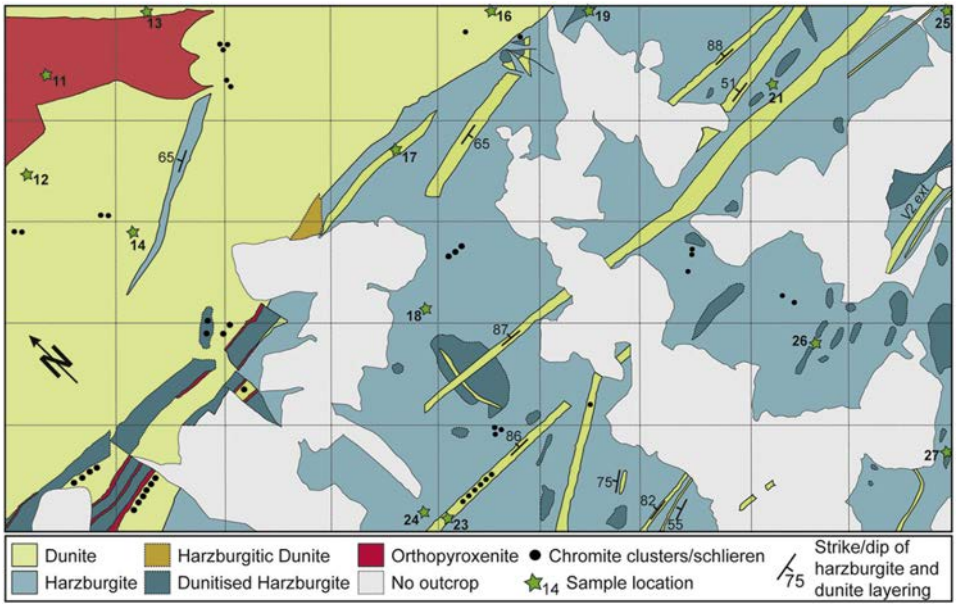

Fig. 1. Sketch map of the lithological relationships in The Viels study area. The horizontal border of this sketch map is oriented 333° and the grid squares are 1 m in length. The thin dunite channel labelled 'V2ext' is the same channel that Sample V2 of O'Driscoll et al. (2012) was sampled from (see text for details).

(e.g., Kelemen, 1990; Büchl et al., 2002, 2004; Alard et al., 2005; Harvey et al., 2006; Bizimis et al., 2007; Warren et al., 2009; Stracke et al., 2011; Burton et al., 2012; Rampone and Hofmann, 2012).

A paucity of accessible exposures of fresh modern-day oceanic peridotites is a major obstacle to a detailed direct assessment of its chemical and isotopic heterogeneity. Abyssal peridotites, commonly presumed to be the residua after partial melting to produce mid-ocean ridge basalts (MORB; Dick et al., 1984; Warren et al., 2009; Lassiter et al., 2014; Warren, 2016; Day et al., 2017a), provide one option for the direct study of mantle peridotites. Abyssal peridotites, however, are most frequently collected by ocean dredging, and so field relations amongst different samples are normally poorly constrained, with a few exceptions (e.g., Harvey et al., 2006; Mallick et al., 2015).

Ophiolite peridotites are also useful for studying upper mantle processes. Ophiolites represent slivers of oceanic lithosphere thrust (obducted) onto continental crust at convergent plate margins. Ideally, they preserve both mantle and crustal sections. Ophiolite peridotites provide snapshots of the long-term evolution of the oceanic lithospheric mantle, as known ophiolites range in age from Archaean to as young as ~6 Ma (Büchl et al., 2002; Schulte et al., 2009; Dilek and Furnes, 2011; O'Driscoll et al., 2012, 2015). Ophiolites also have the advantage that they may provide excellent constraints on field relations, including providing spatial and structural context for lithologically diverse mantle rocks. As with most abyssal peridotites, however, ophiolite peridotites are commonly highly serpentinised, and may also have been modified by supra-subduction zone (SSZ) processes (Dilek and Furnes, 2011). Consequently, study of ophiolite peridotites requires either the application of elements that are minimally affected by secondary processes, or elements for which the secondary effects can somehow be circumvented. The absolute and relative abundances of the highly siderophile elements (HSE; Os, Ir, Ru, Pt, Pd, Re), combined with the Re–Os isotope system, have proven useful in this context because mantle peridotites tend to be characterised by much higher concentrations of these elements than both crustal rocks and fluids whose recycling can strongly modify the compositions of lithophile trace elements and Sr–Nd–Hf–Pb isotope systematics (cf., Becker and Dale, 2016).

Application of the HSE and Os isotopes to ophiolitic mantle samples has potential to provide insights into the distribution and the range of length-scales over which compositional heterogeneities occur in the oceanic mantle. The mantle section of the ~492 Ma Shetland Ophiolite Complex (SOC; Fig. S1) is a valuable locality to examine in detail due to excellent exposure of the mantle section and the context provided by previous work on Os isotopes and HSE abundances (e.g., O'Driscoll et al., 2012; Prichard et al., 2017).

The aim of this study is to advance understanding of mantle chemical and isotopic heterogeneities over length-scales of several metres, i.e., at the outcrop scale, and tie these phenomena to lithological variations observed in the field. We link our metre-decametre scale observations to grain-scale controls by considering the distribution and HSE compositions of base-metal sulphides, platinum-group element (PGE) phases, and Cr-spinel in relevant lithologies.

2. Geological setting and sample selection

The ~492 Ma SOC represents Iapetus Ocean lithosphere, and is one of numerous tectonic ophiolite fragments now dispersed along the length of the Caledonian orogen from NW Norway, through the UK and Ireland, Newfoundland, and as far south as the Appalachians in the eastern USA (Spray and Dunning, 1991; Chew et al., 2010). The SOC is considered to have been obducted onto Laurentia at ~470 Ma (Flinn, 2001). Although overlying components of the ophiolite are missing or poorly exposed (e.g., the sheeted dyke complex), the mantle section is extensive and well-preserved (Derbyshire et al., 2013). The mantle section comprises serpentinised harzburgite (~70 vol.%), with numerous dunite layers and lenses, and less abundant chromitites and pyroxenites (Fig. S1; Flinn, 2001). Chromitite seams occur encased in dunite sheets and pods, a relationship that has previously been explained due to formation of chromitite during high degrees of melt–rock reaction in channels of focused melt flow (O'Driscoll et al., 2012; Derbyshire et al., 2013). In the case of the SOC, melt extraction likely occurred in a forearc supra-subduction zone (SSZ) setting (Crowley and Strachan, 2015).

A ~45 m^2 area situated 200 m below the petrological Moho at "The Viels" (Fig. S1), was selected for study due to the good expo-

Table 1
Re–Os isotopes and highly siderophile element abundances for The Viels peridotites.

Sample	Lithology	MgO (wt.%)	Al_2O_3 (wt.%)	Os	Ir	Ru	Pt	Pd	Re	$^{187}Re/^{188}Os$	$\pm 2\sigma$	$^{187}Os/^{188}Os$	γOs (492 Ma)	T_{RD} age	T_{MA} age
Un-13-11	Orthopyroxenite	37.3	1.37	0.142	0.349	0.765	0.543	0.308	0.0075	0.25	0.008	0.12839	2.1	0.1	–
Un-13-12	Dunite	47.8	0.21	3.334	2.779	6.777	3.315	9.265	0.047	0.0682	0.0020	0.12430	0.0	0.5	0.50
Un-13-13	Dunite	48.6	0.13	8.173	5.625	11.13	0.628	0.438	0.024	0.0142	0.0004	0.12611	1.9	0.2	0.15
Un-13-14	Dunite	48.3	0.17	8.371	6.310	14.00	2.817	0.536	0.049	0.0280	0.0008	0.12670	2.2	0.1	0.06
Un-13-16	Dunite	48.9	0.09	1.805	3.453	6.949	3.011	0.403	0.052	0.1377	0.0041	0.12410	−0.6	0.6	0.68
Un-13-17	Dunite	48.7	0.26	2.012	5.616	7.453	5.006	2.917	0.102	0.2440	0.0073	0.13495	7.5	–	–
Un-13-18	Harzburgite	45.4	0.55	5.215	4.669	8.726	7.014	15.25	0.767	0.7090	0.0213	0.13128	1.4	0.2	0.81
Un-13-19	Harzburgite	46.5	0.46	3.531	2.843	6.178	4.070	0.489	0.027	0.0368	0.0011	0.11906	−4.0	1.2	1.31
Un-13-20	Harzburgite	46.1	0.50	3.475	3.184	6.723	7.692	1.631	0.015	0.0210	0.0006	0.12667	2.3	0.1	0.07
Un-13-21	Harzburgite	44.4	0.72	2.868	1.588	6.509	6.163	2.160	0.0052	0.0088	0.0003	0.12640	2.1	0.1	0.11
Un-13-23	Dunite	48.0	0.34	4.747	4.478	9.970	9.703	10.42	1.384	1.407	0.0422	0.14163	5.1	–	0.86
Un-13-24	Harzburgite	44.8	0.64	1.771	1.879	5.516	4.475	1.219	0.112	0.0306	0.0009	0.12659	2.2	0.3	0.08
Un-13-25	Harzburgite	45.3	0.61	4.477	3.427	7.621	9.900	2.320	0.0077	0.0082	0.0002	0.12710	2.7	0.0	0.00
Un-13-26	Harzburgite	46.3	0.37	2.396	1.503	7.846	2.056	2.024	0.059	0.1188	0.0036	0.12584	0.9	0.3	0.27
Un-13-27	Harzburgite	45.6	0.58	3.964	2.716	7.294	10.74	2.862	0.0035	0.0042	0.0001	0.11946	−3.5	1.1	1.14
V1	Dunite	48.2	0.30	5.886	3.885	12.04	4.571	4.170	0.084	0.0690	0.0021	0.12649	1.3	0.4	0.02
V2	Dunite	45.6	1.22	41.68	38.40	56.11	407.4	644.9	14.84	1.7194	0.0516	0.14178	2.7	–	–
V3	Harzburgite	45.3	0.36	3.657	3.849	6.018	5.764	9.870	0.087	0.1148	0.0034	0.12306	−1.8	0.9	0.56
V4	Dunite	47.0	0.13	5.053	4.959	8.094	5.079	9.149	0.070	0.0664	0.0020	0.12079	−3.3	1.2	0.82
V6	Harzburgite	45.7	0.28	2.614	2.626	3.846	3.499	3.182	0.033	0.0617	0.0019	0.11821	−5.3	1.6	1.18

Highly siderophile element abundances in $ng\,g^{-1}$.
Samples V1, V2, V3, V4 and V6 from O'Driscoll et al. (2012).
Uncertainty (2σ) on $^{187}Os/^{188}Os$ is ~0.2%.

sure there of the major mantle lithologies in the SOC (harzburgite, dunite, orthopyroxenite) (Fig. 1; see also Fig. S1). About ~60% of the mapped area comprises harzburgite (Fig. 1, Figs. S2a, S2b). The harzburgite retains 20–30 vol.% fresh olivine, and rarely, fresh orthopyroxene, but is otherwise serpentinised. Chromian-spinel is present in the harzburgite in accessory (<1 vol.%) abundances. Rarely, diffuse stringers of base-metal sulphides cut the harzburgite (e.g., sample Un_13_18). A thick (>5 m) dunite sheet intrudes in the northern portion, itself intruded by a completely serpentinised orthopyroxenite body (e.g., Figs. 1, S2c). The thick dunite sheet typically does not contain obvious sulphide (Un_13_13 is an exception), but Cr-spinel occurs in clots and diffuse schlieren, as well as being disseminated throughout. The thick dunite sheet contains harzburgite autoliths and has a complex outer margin on its southwestern side, comprising dunitised harzburgite and multiple orthopyroxenite selvedges (Fig. 1). The harzburgite hosts multiple thin (~10–20 cm) sheets of dunite containing 1–5 vol.% visible base-metal sulphide. Compared to the harzburgites, these dunites have enhanced abundances of Cr-spinel (Un_13_17 and Un_13_23; e.g., Fig. S2d). Ubiquitously they contain orthopyroxene autocrysts and, less commonly, cm-sized fragments of harzburgite. The thick and thin dunite sheets are oriented sub-parallel to one another, broadly striking E–W. Dunites are generally less serpentinised than harzburgites and may contain up to 50 vol.% fresh olivine. There are numerous irregularly-shaped (sub m^2) areas of 'dunitised' harzburgite (see Fig. 1 and Fig. S2b; e.g., Un_13_19 and Un_13_27). These zones comprise harzburgite containing irregular and diffuse volumes of dunite, and in many cases have long axes oriented E–W. The dunite incorporates orthopyroxene pseudomorphs from the harzburgite, and contains cm-sized clusters of Cr-spinel grains. Notably, the thin dunite bodies cross-cut the dunitised harzburgite zones (Fig. 1).

We report HSE abundances and Re–Os isotopic (Table 1) data for fifteen new samples from The Viels (eight harzburgites, six dunites and one orthopyroxenite) and discuss these together with data for five additional samples previously reported (V1, V2, V3, V4, V6; O'Driscoll et al., 2012), all of which were located 1–2 m from the SE corner of The Viels study area (Fig. 1). Table 1 contains the details of sample numbers and lithologies.

3. Analytical techniques

3.1. Major and trace element abundance measurements

Whole-rock major element concentrations were obtained by X-ray fluorescence (XRF) analysis using a PANalytical 2404 X-ray fluorescence vacuum spectrometer at Franklin and Marshall College, Lancaster, PA (USA), following the procedures outlined in Boyd and Mertzman (1987). Further details of the XRF method are provided in the Supplementary Materials.

Trace-element abundances were determined at the Scripps Isotope Geochemistry Laboratory (SIGL), Scripps Institution of Oceanography (USA), using methods described by Day et al. (2017a). One hundred milligrammes of powder was precisely weighed and then digested in a 1:4 mixture of Teflon-distilled HNO_3:HF for >72 hrs at 150 °C on a hotplate. Rock standards (BHVO-2, BIR-1, BCR-2, AGV-2, GP13, DTS-2b) and total procedural blanks were prepared along with the samples. After drying down and sequential HNO_3 dry-down steps to break-down fluorides, clear sample solutions were diluted by a factor of 5000 in 2% HNO_3 and doped with a 1 $ng\,g^{-1}$ In solution to monitor instrumental drift. Solutions were measured using a *Thermo Scientific iCAPq c* quadrupole inductively coupled plasma mass spectrometer in standard mode. Reproducibility of the reference materials was generally better than 5% (RSD) for basaltic and peridotite standards, and element abundances were generally within error (1σ SD) of recommended values (see Table S2).

3.2. Rhenium–osmium isotope and HSE abundance measurements

Osmium isotope and HSE abundance analyses were performed at the University of Maryland, College Park (USA). Precisely weighed homogenised powders were digested in sealed borosilicate Carius tubes, with isotopically enriched multi-element spikes (^{99}Ru, ^{105}Pd, ^{185}Re, ^{190}Os, ^{191}Ir, ^{194}Pt), and 12 mL of a 1:2 mixture of multiply Teflon-distilled HCl and HNO_3 purged of Os by repeated treatment and reaction with H_2O_2. Samples prepared in Carius tubes were digested to a maximum temperature of 270 °C in an oven for 72 hrs. Osmium was triply extracted from the acid using CCl_4 and then back-extracted into concentrated

HBr (Cohen and Waters, 1996), prior to purification by microdistillation (Birck et al., 1997). Rhenium and the other HSE were recovered and purified from the residual solutions using standard anion exchange separation techniques (Becker et al., 2006; Day et al., 2016).

Isotopic compositions of Os were measured in negative-ion mode on a *ThermoFisher Triton* thermal ionisation mass spectrometer at the University of Maryland. Rhenium, Pd, Pt, Ru and Ir were measured using a *Cetac Aridus II* desolvating nebuliser coupled to a *Thermo Fisher Element 2* ICP-MS. Offline corrections for Os involved an oxide correction, an iterative fractionation correction using $^{192}Os/^{188}Os = 3.08271$, a ^{190}Os spike subtraction, and finally, an Os blank subtraction. Precision for $^{187}Os/^{188}Os$, determined by long-term repeated measurement of the UMCP Johnson–Matthey standard, was better than ±0.2% (2 SD; 0.11378 ±15; $n = 5$). Measured Re, Ir, Pt, Pd and Ru isotopic ratios for sample solutions were corrected for mass fractionation using the deviation of the standard average run on the day over the natural ratio for the element. External reproducibility on HSE analyses was better than 5% for >1 ng g^{-1} solutions and all reported values are blank corrected. The total procedural blanks run with the samples for Carius tubes had $^{187}Os/^{188}Os = 0.161$, with quantities (in picograms) of 1.3 [Re], 14 [Pd], 37 [Pt], 5.8 [Ru], 1.9 [Ir] and 2.4 [Os]. These blanks resulted in negligible corrections to samples (<3%), except for several low-Re samples for which the blank comprised as much as 20% of the total measured Re.

3.3. Electron microprobe and laser ablation ICP-MS measurements

Base-metal sulphides were analysed for the three samples in which they were of sufficiently large grain size and abundance (i.e., Un_13_13, Un_13_18 and Un_13_23). Chromian-spinel compositions were also analysed in these samples. Electron microprobe measurements were carried out at the University of Manchester, using a *Cameca SX 100*. *In situ* laser-ablation ICP-MS analysis of Cr-spinel and sulphides were performed at the University of Maryland using a *New Wave* 213 nm laser-ablation system coupled to an *Element 2* ICP-MS, following the procedure described in O'Driscoll et al. (2012, 2015). Further details of these methodologies are presented in the Supplementary Materials.

4. Results

4.1. Major and lithophile trace element abundances

The Viels major element data are presented in Table S1. The harzburgites and dunites have compositions that are similar to other SOC peridotites, as well as peridotites from the broadly coeval Leka ophiolite, Norway (O'Driscoll et al., 2015). Whole rock Al_2O_3 and SiO_2 are negatively correlated with MgO (Fig. 2a), and Al_2O_3 concentrations (anhydrous corrected) range between 0.4–0.7 wt.% for the harzburgites and 0.1–0.3 wt.% for the dunites. The Viels harzburgites overlap with the low-Al_2O_3/high-MgO end of the array of abyssal peridotite compositions (e.g., Day et al., 2017a), and the dunites extend to higher MgO and lower Al_2O_3 (Fig. 2a). Loss on ignition (LOI) values for The Viels suite range between 10–16 wt.% (average 13 ± 4 wt.%, 2σ). Dunites and harzburgites with higher LOI values tend to exhibit higher (visible) degrees of serpentinisation.

Lithophile trace element abundances of peridotites from The Viels are tabulated in Table S2. Plots of PM-normalised incompatible trace elements, as well plots of Nb/Ta versus Zr/Hf and Sm/Nd versus Nb/Ta are presented in Fig. S3. Broadly, samples are depleted in most incompatible lithophile trace elements by one to two orders of magnitude with respect to PM, similar to Leka ophi-

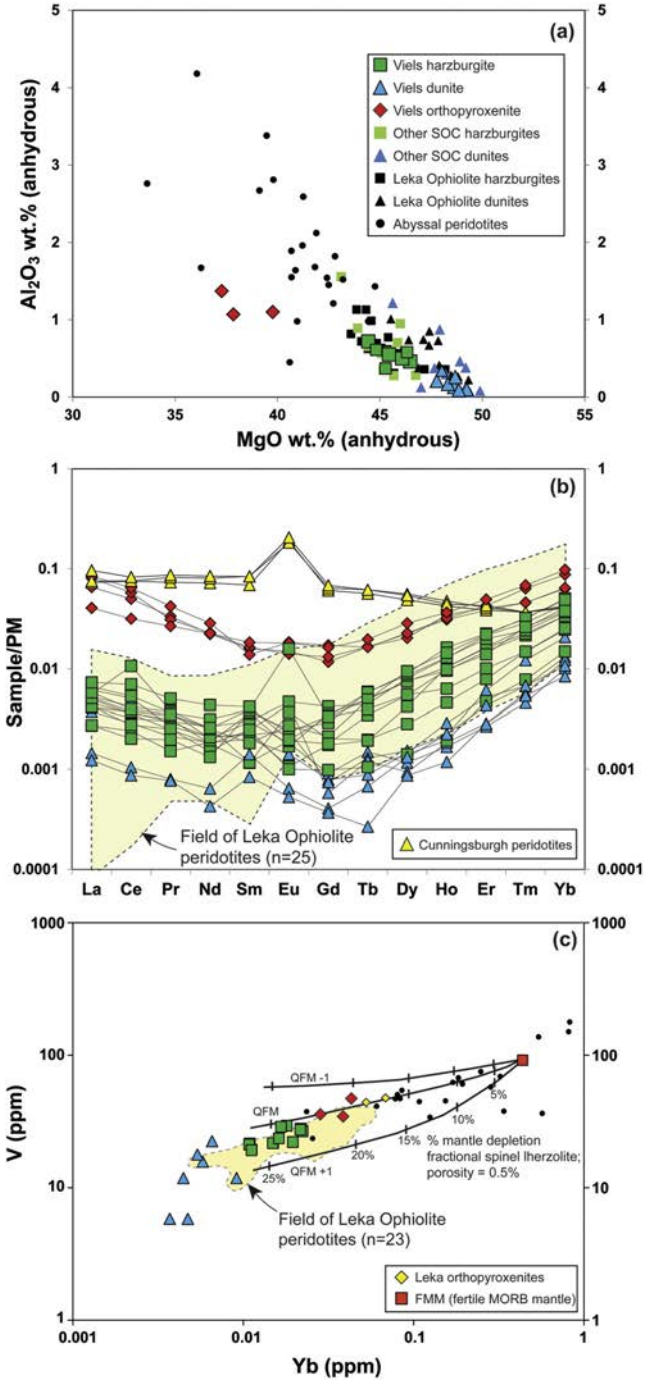

Fig. 2. (a) Al_2O_3 versus MgO for The Viels samples. Also shown are data for other SOC peridotites (O'Driscoll et al., 2012), for the Leka Ophiolite peridotites (O'Driscoll et al., 2015) and for a global compilation of abyssal peridotites (Day et al., 2017a). (b) Primitive mantle normalised REE abundances of The Viels harzburgites, dunites and orthopyroxenite (Un_13_11). Also shown are the range of compositions of 25 Leka Ophiolite peridotites (shaded field) and three dunites of purported mantle origin on the Shetland mainland (yellow triangles; Day et al., 2017b). Normalisation values are from McDonough and Sun (1995). (c) Vanadium versus Yb for The Viels peridotites. The modelled melt extraction and oxygen fugacities (QFM, quartz–magnetite–fayalite buffer) are from Pearce and Parkinson (1993) and Parkinson and Pearce (1998). The tick marks represent 5% melt removal increments. The theoretical composition of fertile MORB mantle is shown as FMM (Pearce and Parkinson, 1993). Also shown are the range of Leka Ophiolite peridotite compositions and the global compilation of 65 abyssal peridotite compositions (of which 22 are shown here) of Day et al. (2017a and references therein). The latter compilation includes 36 Gakkel Ridge samples, 7 MAR samples (4 Kane, 3 MARK), 20 Indian Ridge samples (5 CIR, 14 SWIR) and 2 Pacific Ocean samples (Hess Deep). (For interpretation of the colours in the figure(s), the reader is referred to the web version of this article.)

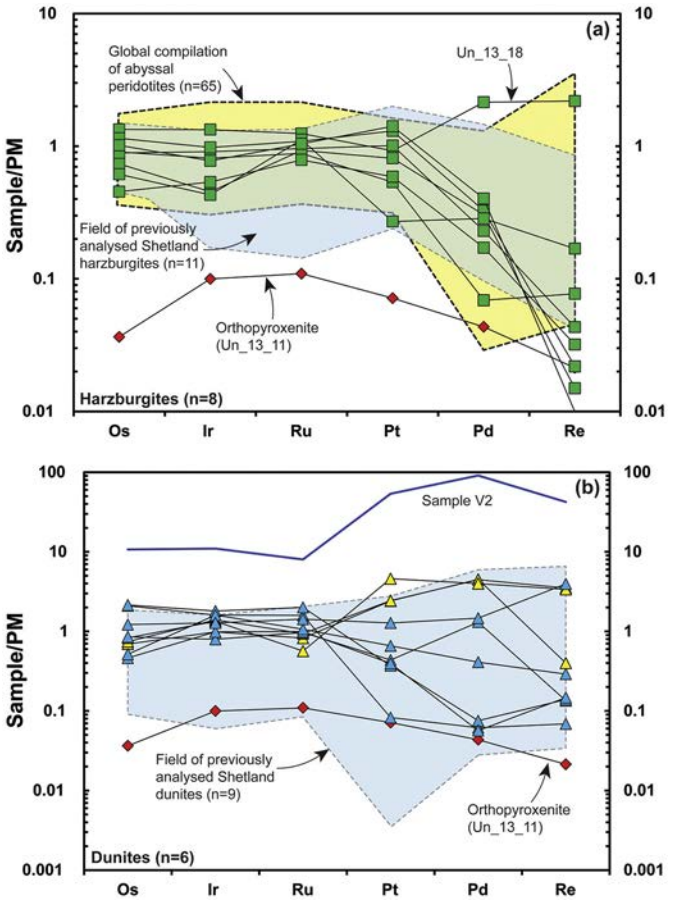

Fig. 3. Primitive mantle normalised (after Becker et al., 2006) highly siderophile element (HSE) patterns for (a) The Viels harzburgites and orthopyroxenite, with highlighted fields for the previously reported Shetland Ophiolite Complex (SOC) harzburgites (O'Driscoll et al., 2012) and the Day et al. (2017a) abyssal peridotite compilation. (b) SOC dunites and orthopyroxenite, with the field for previously analysed SOC dunites (O'Driscoll et al., 2012) shown by the shaded field. Also shown is the sulphide-rich dunite sample V2 from O'Driscoll et al. (2012) and the three southern Shetland dunites (Cunningsburgh peridotites) reported in Day et al. (2017b). The symbols used are the same as in Fig. 2.

olite mantle samples (O'Driscoll et al., 2015). The Viels dunites are more depleted in most elements than the harzburgites, with the orthopyroxenite being relatively enriched compared to both harzburgites and dunites (Fig. S3a).

Peridotites from the SOC mantle are depleted in the light rare earth elements (LREE) relative to the heavy-REE (HREE), with concentrations of the HREE ranging from 0.01 × PM for the dunites, 0.01–0.1 × PM for the harzburgites and ~0.1 × PM for the orthopyroxenite (Fig. 2b). The dunite samples are the most REE-depleted samples of the suite analysed. Both harzburgites and dunites have LREE that are 0.001–0.01 × PM, whilst the orthopyroxenite has LREE ~0.1 × PM. All samples exhibit concave-upward PM-normalised REE patterns (Fig. 2b). Several dunites and harzburgites (e.g., Un_13_15, Un_13_17, Un_13_20) are also characterised by positive Eu anomalies. The Viels peridotites are relatively depleted, particularly in the MREE, compared to rocks interpreted as mantle peridotites in the southern Shetland archipelago (the Cunningsburgh peridotites; Day et al., 2017b). The Viels harzburgites and dunites are similar to Leka peridotites, albeit the latter extend to more depleted LREE and elevated HREE abundances (O'Driscoll et al., 2015).

4.2. Highly siderophile element abundances and ^{187}Re–^{188}Os isotope systematics for bulk samples

Highly siderophile element abundance data for bulk samples are reported in Table 1. Primitive mantle normalised plots of the HSE in the harzburgites and dunites are presented in Figs. 3a and 3b, respectively. The orthopyroxenite (Un_13_11) is plotted on both panels for reference. Also included on these plots are the fields for previously analysed Shetland peridotites (O'Driscoll et al., 2012) and an abyssal peridotite compilation from Day et al. (2017a). The Viels harzburgites have HSE patterns that fall within the range of abyssal peridotites, and within the range of SOC harzburgite compositions previously reported by O'Driscoll et al. (2012; Fig. 3a). Harzburgites have PM-like concentrations of Os, Ir, Ru and Pt, but depletions in Pd and particularly in Re (0.01 × PM). Nearly all of the HSE data plot within the range of concentrations defined by abyssal peridotites.

The HSE concentrations in The Viels dunites are characterised by IPGE (Os, Ir, Ru) and Pt contents similar to those of the harzburgites and PM; they plot within the range of dunites previously measured from the SOC (Fig. 3b). Some dunites from the thick channel (Fig. 1) exhibit depletions in Pd (Un_13_14 and Un_13_16). Rhenium concentrations in the dunites are elevated relative to the harzburgites, typically at levels of ~0.1 × PM. The orthopyroxenite HSE PM-normalised pattern is convex-upward and exhibits depletions of 0.01–0.1 × PM in all of the HSE (Fig. 3b). The HSE pattern for this orthopyroxenite is quite different from HSE patterns for orthopyroxenites reported from the Leka Ophiolite (O'Driscoll et al., 2015), which are characterised by strongly elevated Pt and Pd, relative to the IPGE.

Rhenium–Os isotope data are reported in Table 1, and plotted in Fig. 4a–c. With one exception, the $^{187}Re/^{188}Os$ ratios of The Viels harzburgites are sub-chondritic (<0.4), averaging 0.12 ± 0.24 (1σ; $n = 8$) and span nearly the entire range reported for harzburgites collected across the mantle section of the SOC (O'Driscoll et al., 2012). Harzburgite Un_13_18 has a modestly suprachondritic ratio of 0.709. The $^{187}Re/^{188}Os$ ratios for the dunites are generally more variable, ranging to as high as 1.4 (Figs. 4a, 4b, 4c), and averaging 0.32 ± 0.54 (1σ; $n = 6$). The orthopyroxenite has a $^{187}Re/^{188}Os$ ratio of 0.25. The age corrections necessary to calculate the initial $^{187}Os/^{188}Os$ ratios for these samples are generally minor, due to the comparatively low Re/Os.

Calculated initial γOs values (percent deviation from a chondritic reference composition at 492 Ma) for the harzburgites range from −4.0 to +2.7, and for the dunites range from −0.6 to +7.5 (Fig. 4c). The orthopyroxenite has a γOs value of +2.1. Thus, initial γOs values vary by more than 10 units ($^{187}Os/^{188}Os$ varies by >10%), regardless of Re/Os (Fig. 4c). The two harzburgites with lowest initial γOs values, Un_13_19 and Un_13_27, have corresponding Re depletion model ages (T_{RD}; Shirey and Walker, 1998) of 1.2 to 1.1 Ga, respectively, where T_{RD} ages represent minimum ages based on the assumption of no ingrowth of ^{187}Os in the samples since melt depletion.

4.3. Mineralogical controls on HSE distribution in the SOC peridotites

Mineral compositional data are presented in Table S3. The average Cr# (Cr/Cr + Al) of Cr-spinel in both Un_13_18 and Un_13_23 is 0.61, whilst the value for Un_13_13 is 0.72. Sulphides and base-metal phases are not typically visible in harzburgite hand specimens from The Viels, or in dunites from the ~5 m thick sheet in the northern portion of the area. Exceptions to this are Un_12_13 (dunite) and Un_12_18 (harzburgite), which both contain narrow cross-cutting stringers of pentlandite ($[Fe,Ni]_9S_8$) (Fig. S4). In the narrow dunite channels represented by Un_13_17 and Un_13_23, pentlandite is the dominant sulphide species, along with minor

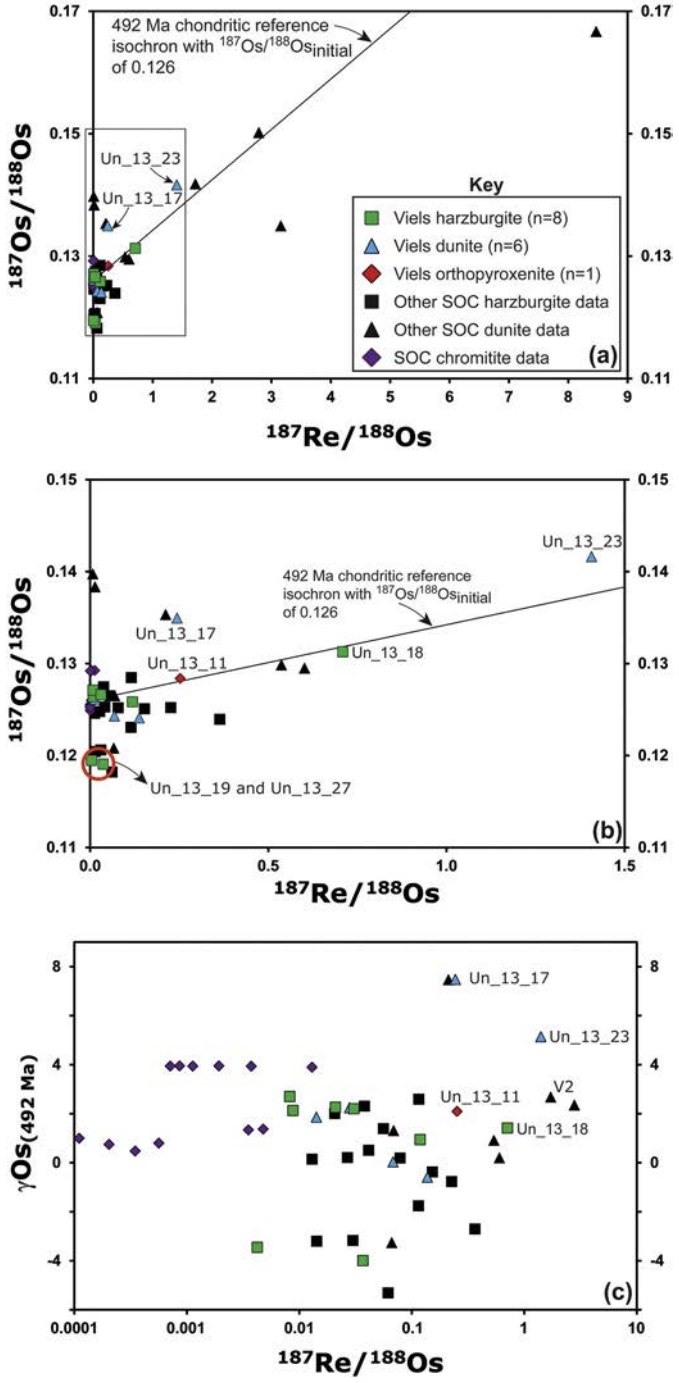

Fig. 4. (a) Plot of $^{187}Re/^{188}Os$ versus $^{187}Os/^{188}Os$ for The Viels peridotites (harzburgites, dunites, orthopyroxenite, as well as previously published SOC data), with a 492 Ma chondritic reference isochron [initial $^{187}Re/^{188}Os$ and $^{187}Os/^{188}Os$ values for chondrite are from Shirey and Walker (1998)]. (b) Close-up of area highlighted in the black square in panel above, showing the distribution of relatively low $^{187}Re/^{188}Os$–$^{187}Os/^{188}Os$ samples. The two samples with relatively low γOs compositions are highlighted. (c) Plot of γOs vs $^{187}Re/^{188}Os$ (see text for discussion).

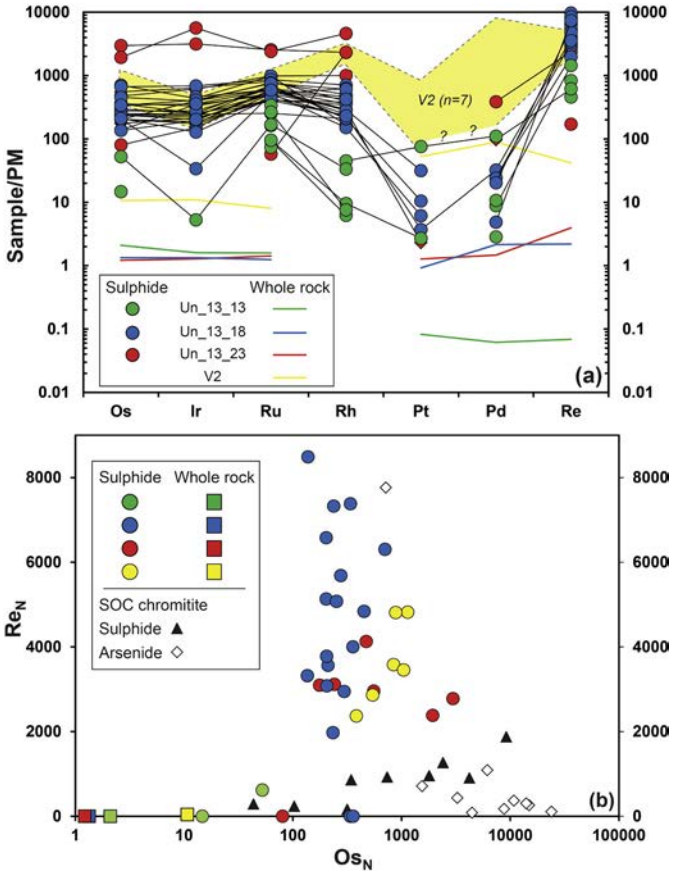

Fig. 5. Primitive mantle normalised (after Becker et al., 2006) highly siderophile element LA-ICP-MS data for sulphides from three of the dunites studied here: Un_13_13, Un_13_18 and Un_13_23. In (a), the primitive mantle normalised HSE patterns are shown together with their whole rock compositions and the range of sulphide compositions for the V2 dunite, the sulphide-rich dunite reported by O'Driscoll et al. (2012). In (b), Re_N versus Os_N values (denoting primitive mantle normalised Re and Os, respectively) are plotted for the three dunites, as well as for Sample V2 (yellow filled circles). Also shown are sulphide and arsenide compositions from the Harold's Grave and Cliff chromitites from O'Driscoll et al. (2012).

heazlewoodite (Ni_3S_2), and is disseminated throughout the samples. Where visible, platinum-group minerals (PGM) are closely spatially associated with sulphides, typically located at the margins of sulphide grains. The dominant PGM observed are sperrylite ($PtAs_2$), with maximum grainsize dimensions up to 2 µm, and irarsite [(Ir,Ru,Rh,Pt)AsS] (see Fig. S4). On PM-normalised HSE plots (Fig. 5a), pentlandites typically have HSE concentrations 100–10000 × PM. Sulphides from Un_13_23 have the highest HSE concentrations. Sulphides from Un_13_18 have lower HSE concentrations, and sulphides from Un_13_13 have the lowest concentrations. The sulphides from all three samples have HSE patterns with relative depletions in Pt and Pd (≈ PM levels). The sulphides also show mild (Un_13_18) to major (Un_13_13) depletions in Ir relative to Os and Ru (Fig. 5a).

Even though pentlandites vary in terms of their relative HSE contents within the same sample, the whole rock HSE abundances of Un_13_13, Un_13_18 and Un_13_23 are accounted for by the abundance of sulphide observed in each of the three samples, with the exception of Pt and Pd. Each of the three samples in question contains approximately 1 vol.% sulphide. For example, Os and Ir concentrations in Un_13_23 can be accounted for by <0.1% by mass of a sulphide fraction with the composition of the most HSE-rich grain analysed by LA-ICP-MS. Similarly, Re concentrations in Un_13_18 and Un_13_23 can be accounted for by ~0.01% by mass of the average Re concentration of the sulphides analysed from these samples. Concentrations of the HSE in Cr-spinel are negligible compared to sulphides, with the exception of Ru, which reaches >1 µg g^{-1} in the Cr-spinel from Un_13_18, and is present in concentrations >100 ng g^{-1} in Cr-spinel from all three analysed samples. Comparison of the sulphide HSE patterns with the whole rock data indicate that the sperrylite and irarsite played a significant role in fixing Pt and Ir contents in the samples. Mineral phases responsible for sequestering the Pd have not been identi-

fied, but Derbyshire et al. (2013) reported a Pd–Fe–Ni alloy at The Viels that could potentially be implicated.

There are additional differences in the HSE compositions of the sulphides from different samples (Fig. 5b). In particular, Re concentrations in Un_13_23 and particularly Un_13_18 sulphides are relatively high, ranging up to ~4 $\mu g\,g^{-1}$. In contrast, Un_13_13 sulphides exhibit Re concentrations that are generally at sub-$\mu g\,g^{-1}$ levels and Os concentrations that are mostly below detection.

5. Discussion

5.1. Serpentinisation and the extent of the SSZ overprint on The Viels peridotites

To consider the extent of chemical and isotopic heterogeneity present in the original oceanic mantle in what is now The Viels locale, it is important to identify the effects of serpentinisation and any SSZ overprint that may have occurred during and subsequent to the extraction of the rocks from the mantle.

The Viels peridotites show similar degrees of serpentinisation and LOI values to abyssal peridotites (Day et al., 2017a), suggesting that low temperature alteration in ophiolitic peridotites may be comparable to some abyssal peridotites. Several studies have concluded that serpentinisation does not strongly modify the primary HSE compositions of ophiolite or abyssal peridotites (e.g., Snow and Reisberg, 1995; O'Driscoll et al., 2012, 2015; Day et al., 2017a). Further, relative similarities of the HSE abundances and Os isotope compositions of The Viels peridotites to other SOC mantle peridotites, and to the global abyssal peridotite database (Day et al., 2017a), suggests that serpentinisation has not significantly affected the abundances of these elements. The dunites with the highest Re concentrations also contain high Re/Os sulphides (Fig. 5b), so their $^{187}Re/^{188}Os$ compositions are likely not a result of serpentinisation or seafloor alteration, given the limited Re available (e.g., Re concentrations in seawater are on the order 7–8 $ng\,kg^{-1}$; Anbar et al., 1992). Some of The Viels peridotites are up to 80 vol.% serpentinised, and elevated concentrations of highly fluid mobile elements Sr, U and Pb in certain samples (see Fig. S3a) suggest that seawater-related alteration has influenced the abundances of some lithophile trace elements. However, comparisons of most other lithophile trace elements, including the REE, with abyssal peridotite concentrations and with other peridotites (e.g., O'Driscoll et al., 2015; Day et al., 2017a) suggest that low temperature alteration was not otherwise significant in modifying the compositions of The Viels peridotites.

Subduction-related processing is more likely to have led to modifications of The Viels peridotites that would obscure the original characteristics of this section of the palaeo-oceanic mantle. Numerous channels and schlieren of dunite, pyroxenite and chromitite attest to the importance of melt extraction, percolation and melt–rock reaction in the formation of the SOC mantle (O'Driscoll et al., 2012). Studies of ophiolite peridotites have concluded that these channels are common products of SSZ processes (e.g., Kelemen, 1990; Kelemen et al., 1992; Büchl et al., 2002, 2004; O'Driscoll et al., 2012). The compositions of Cr-spinel in The Viels dunites (e.g., Cr# of 0.61–0.72) point to relatively high degrees of melt–rock interaction in the dunite channels, consistent with a SSZ setting. All of The Viels samples, but especially the dunites and orthopyroxenite, show concave-upwards primitive mantle-normalised REE abundance patterns, i.e., with lower MREE than LREE or HREE. These are similar patterns to those observed in many ophiolite peridotites (Bodinier and Godard, 2003) and also in Izu-Bonin peridotites, where it was suggested that subduction-zone melt infiltration occurred, characterised by relatively elevated LREE compositions, and might be responsible (cf. Johnson and Dick, 1992; Parkinson and Pearce, 1998).

The relationships of Ti and V to Yb may provide information on the depth of mantle melting and the redox conditions under which melting occurred (Pearce and Parkinson, 1993; Parkinson and Pearce, 1998). The array of compositions in Ti–Yb space suggests that all Viels peridotites conform to a melting regime at relatively shallow mantle depths (Fig. S3c), i.e., melt extraction in the spinel stability field. The plot of V versus Yb shows that The Viels peridotites define a steeper array than the modelled fractionation trends (Fig. 2c), an observation also made for the Leka Ophiolite peridotites by O'Driscoll et al. (2015). The relationship between V and Yb suggests that The Viels harzburgites formed by ~25% partial melting under oxygen fugacity conditions approximately along the QFM buffer, according to the modelled fractionation trends of Pearce and Parkinson (1993). The Viels dunites are depleted with respect to these elements, compared to abyssal peridotites, consistent with fluid-enhanced SSZ melting. The Viels harzburgite V–Yb compositions overlap with those of the most depleted abyssal peridotites, so the degree to which they have been affected by SSZ melt extraction is more ambiguous. Variation is also observed in the Sm/Nd ratio (0.15–0.91) of the harzburgites (Fig. S3d), suggesting that if subduction zone melting has affected these rocks, it has not done so uniformly.

5.2. Melt–rock reaction and sulphide mobilisation in dunite channels

The Os isotope compositions and HSE abundances of the dunite samples indicate different stages of melt–rock reaction at The Viels. There are thin (<10 cm wide) sulphide-rich channels that incorporate harzburgite fragments and orthopyroxene autocrysts. The two analysed dunite channels of this type (Un_13_17 and Un_13_23) do not show significant depletions in Pd. Their initial γOs values of +7.5 and +5.1 are also radiogenic compared to peridotites from the SOC. Although Un_13_18 is ostensibly a harzburgite, its HSE abundances appear to be largely controlled by thin stringers of sulphides (Fig. 3a), so it is likely that at least the Pd and Re in this rock were concentrated by a mechanism similar to that which acted on the thin dunite channels. Un_13_18 has the most Pd of all The Viels whole rock samples (~15 $ng\,g^{-1}$). The sulphide- and Cr-spinel-rich dunite reported from The Viels area by O'Driscoll et al. (2012; sample V2) is approximately 30 cm thick and contains >1 $\mu g\,g^{-1}$ Pt + Pd, suggesting that it also belongs to the group of thin dunite channels. Sample V2 was collected approximately three metres to the south of the studied area, from what is likely the southeastern extension of one of the thin dunite channels mapped in Fig. 1. The initial γOs value of V2 is +2.7, and it contains sulphides with similar HSE abundances and Re/Os ratios to those in Un_13_23. In contrast to the thin channels, the thick (~5 m wide) channel that dominates the northern part of the studied section does not typically contain visible sulphides, shows marked depletions in Pd, and has relatively low initial Os isotope compositions (i.e., Un_13_12, Un_13_13, Un_13_14, Un_13_16; initial γOs values of −0.6 to +2.2).

The stark contrast between the thick and thin dunite channels suggests that the different HSE and Os isotope characteristics at The Viels are controlled by the presence of multiple populations of base-metal sulphide, with variable HSE abundances, including Re/Os, and initial $^{187}Os/^{188}Os$ (see also Prichard et al., 2017). The two groupings of dunite channels are interpreted as reflecting greater or lesser amounts of melt through-flow and variable retention of melt during melt–rock reaction. The thin dunite channels (e.g., Un_13_18 and Un_13_23), characterised by a relatively large range in Re/Os ratios (Figs. 4c, 5b) and greater enrichment in the PPGE than IPGE, are more 'fertile', reflecting inefficient melt re-

moval during melt–rock reaction. Melt through-flow in these conduits was therefore probably short-lived, so that sulphides formed from melt–rock reaction were frozen *in situ*. By contrast, the thick dunite channel (e.g., Un_13_12, Un_13_14 and Un_13_16) has depleted Pt and Pd in bulk samples, and a sulphide population with relatively low concentrations of HSE and low Re/Os (e.g., Un_13_13). This dunite body, therefore, likely represents a major conduit through which significant host-rock depletion and more protracted melt through-flow occurred, to explain the greater depletion of Pd, Re and lower Re/Os, as well as the higher Cr# of the Cr-spinels (0.72). Early-formed sulphides were transported away and melt through-flow operated in the centre of the conduit, so that further melt–rock reaction and sulphide generation did not occur. In support of this interpretation, the Re/Os of sulphides from Un_13_13 are similar in composition to sulphides and arsenides measured in the SOC podiform chromitites (see Fig. 5b). Chromitites likely form during relatively high degrees of melt–rock reaction in SSZ ophiolite settings (e.g., Arai and Yurimoto, 1994; Derbyshire et al., 2013), and it is within thick (metre-scale) dunite channels that the largest podiform chromitites in the SOC are found.

Field evidence is inconsistent with the dunite channels being older than any of the surrounding The Viels mantle. Although cross-cutting relationships are not observed between any of the dunite channels (Fig. 1), they are oriented almost identically to the thick dunite sheet, suggesting formation under a similar tectonic regime. In addition, the lithophile trace element characteristics of the different dunites are similar, as discussed above, and we argue that all exhibit a SSZ overprint (e.g., Figs. 2b, 2c). A more likely scenario, given the large range of Re/Os in some sulphide populations (e.g., Un_13_18), is that the percolating melts that formed the thin dunite channels and stringers accessed and selectively removed Re and more radiogenic Os from older sulphides or HSE-rich phases with high, long-term Re/Os (see section 5.4 below). Un_13_18 and Un_13_23 both yield model (T_{MA}) ages >800 Ma (Table 1) (where T_{MA} model ages are obtained by extrapolating present day $^{187}Os/^{188}Os$ back in time using the measured Re/Os, to its intersection with the isotopic evolution of a chondritic reference). Given that the T_{MA} age is calculated relative to a chondritic composition, in a conduit where mixing of Os from older and younger components occurred, 800 Ma is probably a minimum age estimate.

5.3. Insights into the pre-SSZ oceanic mantle at The Viels

Excluding dunitised harzburgites, The Viels harzburgite suite has a slightly suprachondritic average initial γOs value of $+1.9 \pm 0.6$ (1σ; $n = 6$). By comparison, harzburgites throughout the SOC are characterised by an average initial γOs value of -0.5 ± 3.4 (1σ, $n = 15$; O'Driscoll et al., 2012), highlighting the relative isotopic heterogeneity of harzburgites regionally, as well as the homogeneity at The Viels locality. If the two dunitised harzburgites with low initial γOs compositions are included, the average γOs value of The Viels harzburgite suite is $+0.5 \pm 2.7$ (1σ; $n = 8$). The combined data for The Viels harzburgite suite then has an average γOs value that is the same as, or only marginally higher than, harzburgites from other Phanerozoic ophiolites including the ~497 Ma Leka ophiolite ($+0.2 \pm 2$, 1σ, $n = 16$; O'Driscoll et al., 2015) and the ~90 Ma Troodos ophiolite ($+0.25 \pm 3.4$, 1σ, $n = 14$; Büchl et al., 2002, 2004).

The Viels harzburgites are also similar to abyssal peridotites in terms of both their HSE abundances and Os isotopic compositions, an observation that suggests SSZ-related melt percolation has had little or no effect on the Os isotopes or HSE abundances of the harzburgites. Therefore, even though there is evidence that at least some of the lithophile trace elements (e.g., LREE) in The Viels harzburgites may have been modified by the passage of SSZ melts, their HSE abundances and Os isotope compositions probably represent the unmodified composition of the Iapetus oceanic mantle at ~492 Ma, prior to serpentinisation and obduction. It follows that the HSE are sensitive recorders of melt extraction and depletion events in the upper mantle. This point is illustrated by Fig. 6a, where Pd/Ir is plotted against $(Nd/Yb)_{PM}$ for The Viels peridotites, and compared with a global abyssal peridotite compilation (Day et al., 2017a). The primitive-mantle normalised Nd/Yb ratio is used as an index of melt depletion, with lower values signifying greater degrees of melt extraction. In oceanic peridotites, higher values might suggest melt percolation or refertilisation. Compared to primitive mantle values, The Viels samples are all highly depleted with respect to the REE, but exhibit a range of Pd/Ir (<0.1 to 3.3), suggesting that HSE abundances were locally controlled by a metasomatic process capable of mobilising and precipitating sulphides (see also Fig. S5), but not significantly refertilising The Viels mantle with respect to incompatible lithophile trace elements. Most of The Viels harzburgites show pronounced depletions of Pd and Re, and Pt to a lesser extent, suggesting that they have undergone significant melt depletion. However, Un_13_18 has a Pd/Ir ratio of 3.3, but a γOs of +1.4 consistent with sulphide metasomatism, likely during SSZ processing, fractionating Pd without strongly modifying the Os isotope composition of The Viels mantle. Indeed, no obvious correlation is observed between γOs and $(Pd/Ir)_{PM}$ (Fig. 6b).

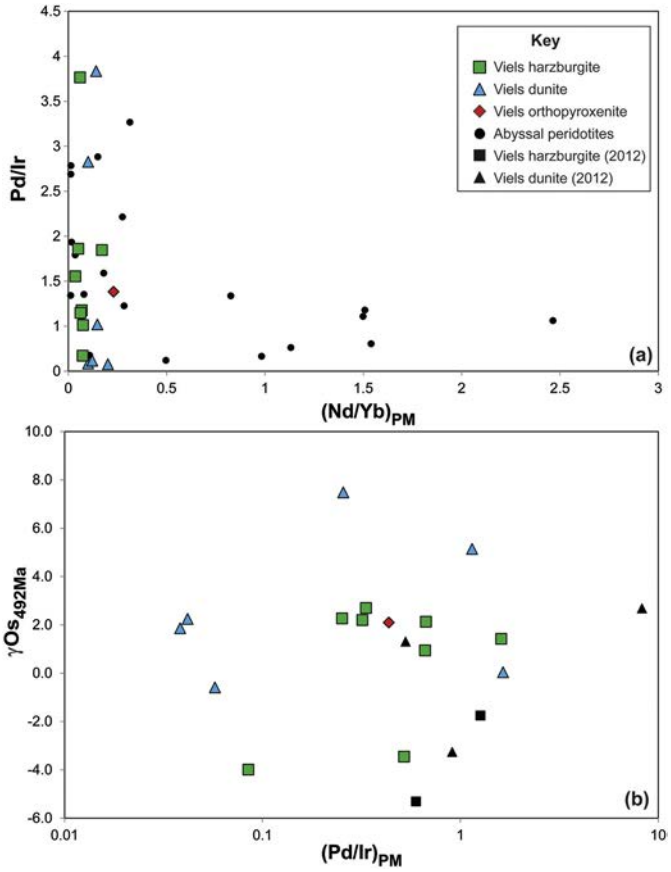

Fig. 6. Plots of (a) Pd/Ir versus $(Nd/Yb)_{PM}$ and (b) γOs versus $(Pd/Ir)_{PM}$. See text for further discussion of these plots.

Within a 45 m^2 area, The Viels harzburgites have a similar range in initial γOs as exists in harzburgites across the entire mantle section exposed on the islands of Unst and Fetlar (Fig. 4c). The presence of harzburgites with Proterozoic T_{RD} ages is not uncommon in Phanerozoic ophiolites, and has previously been attributed to Re loss during melt extraction prior to magmatic pro-

cessing at the time of ophiolite formation (e.g., Schulte et al., 2009; O'Driscoll et al., 2012). The Viels data suggest that Os isotopic heterogeneities in mantle harzburgites occur over sub-metre to metre length-scales in the oceanic mantle. An important finding of this study is that almost the entire range of HSE abundances and especially Os isotopic heterogeneity recorded in the global database for abyssal peridotites can be found at an outcrop scale in the SOC.

5.4. Evidence for a grain-scale control on refractory domains in The Viels mantle

Two of The Viels harzburgites (Un_13_19 and Un_13_27) have relatively low γOs values that yield T_{RD} ages $\geq$1.1 Ga. Two other harzburgites (V3, V6; O'Driscoll et al., 2012) within a metre of the bounds of the area shown in Fig. 1 also have subchondritic γOs, in the case of V6 yielding a T_{RD} age of ~1.6 Ga. Of note, these four harzburgites were all sampled from zones of 'impregnated' or dunitised harzburgite (Figs. 1, S2b). Unlike the dunite channels discussed above, porous melt percolation appears to have occurred in these zones. Although dunitised, the major and lithophile trace element characteristics of these rocks are more consistent with harzburgite rather than dunite compositions (Table 1), suggesting limited geochemical modification due to melt–rock reaction processes, as occurred in the dunite channels. Furthermore, at least one of the dunitised harzburgite patches is cross-cut by a thin dunite sheet, implying that their formation predates those of the dunite bodies (Fig. 1). The dunitised harzburgite patches have long axes oriented in the same direction as the dunite channels (Fig. 1), suggesting a similar SSZ-related origin.

Refractory domains in The Viels mantle are only revealed in harzburgites that have experienced melt percolation and modification. One implication of this observation is that porous melt through-flow has not modified the low Os isotopic compositions sufficiently to obscure these domains. Instead, the dunitisation process appears to accentuate the refractory domains, given that unmodified harzburgites at The Viels exhibit nearly-chondritic γOs. We suggest that SSZ processes operated on harzburgitic mantle in which the IPGE and PPGE were controlled by different PGM phases, leading to preferential retention of highly refractory Os, Ir, Ru-rich PGM. A growing body of literature suggests that Os isotopic heterogeneities, as well as HSE abundances, in the oceanic mantle are controlled at the grain-scale, by Os-rich members of the PGM family, such as laurite (RuS_2) or Os–Ir alloys (see Alard et al., 2005; Walker et al., 2005; Luguet et al., 2007; Lorand et al., 2010; and reviews in González-Jiménez et al., 2014; Lorand and Luguet, 2016, and O'Driscoll and González-Jiménez, 2016). The PGM can exist as inclusions in olivine or especially in Cr-spinel crystals, and thus remain relatively undisturbed by melt extraction. By contrast, Pt and Pd (and Re) can be associated with base-metal sulphides that occupy interstitial positions in mantle peridotites (e.g., Fig. S4; Harvey et al., 2011), and therefore, be mobilised with the sulphide fraction during high degrees of partial melting, or through-flow of sulphide undersaturated melt, allowing the residue to evolve with a less radiogenic $^{187}Os/^{188}Os$ composition compared to unmodified mantle.

The only way that melt percolation at ~492 Ma in The Viels mantle could have revealed refractory domains with T_{RD} ages of 0.9–1.6 Ga (5 samples) is if PGM with low initial Os isotope compositions already existed in these samples at the time of SSZ-processing. There is evidence from studies of other ophiolites that such PGM exist. In particular, ophiolitic dunites and chromitites have populations of PGM characterised by relatively low $^{187}Re/^{188}Os$ and with significant variation in $^{187}Os/^{188}Os$ (e.g., Walker et al., 1996; Pearson et al., 2007; Shi et al., 2007; González-Jiménez et al., 2014). In many instances, chromitites contain PGM whose $^{187}Os/^{188}Os$ ratios yield T_{RD} ages significantly older than the purported age of the ophiolite within which they are found (e.g., Shi et al., 2007). However, such phases are not commonly described from the host peridotites. If porous melt–rock reaction selectively removed high Re/Os phases from irregularly-shaped volumes of The Viels mantle, low initial Os isotope compositions could have been revealed in the dunitised harzburgite represented by samples Un_13_19, Un_13_27, V3 and V6. There is evidence that such sulphides were mobilised in the thin dunite channels (Fig. 5b), so assuming that the dunitisation of the harzburgites and the dunite channels all formed during SSZ-related melt percolation through the SOC mantle, the case can be made that the dunitised harzburgites may have had Os isotope compositions closer to the remainder of The Viels suite (i.e., Un_13_18, Un_13_20, Un_13_21, Un_13_24, Un_13_25, Un_13_26 and Un_13_27) prior to 492 Ma. The lack of a correlation between γOs and $(Pd/Ir)_{PM}$ supports the presence of PGM at this time (Fig. 6b), so that the HSE were variably mobilised by sulphide metasomatism.

Prichard et al. (2017) report LA-ICP-MS data for PGM in the nearby (~1 km) Harold's Grave chromitite (see Fig. S1). Several PGM grains reported in that study yield relatively low initial $^{187}Os/^{188}Os$ ratios and correspondingly old (Proterozoic) T_{RD} ages. In light of the arguments above, it is noteworthy that the PGM that exhibit old T_{RD} ages reported by Prichard et al. (2017) are phases containing enhanced Os abundances (i.e., laurite and native Os), showing that such phases exist in the SOC and may also be responsible for controlling the heterogeneities observed in The Viels peridotites. By extension, we suggest that ancient (Proterozoic) refractory domains in the oceanic mantle more generally may be controlled at the grain-scale for Os isotopes.

6. Conclusions

The ~492 Ma Shetland Ophiolite Complex offers the opportunity to assess lithological and chemical heterogeneities present on centimetre–metre scales in the oceanic mantle. The relatively small (~45 m^2) area studied at The Viels contains an equivalent range of chemical heterogeneity with respect to Os isotopes and HSE abundances as the entire (~300 km^2) SOC mantle section. Despite pervasive serpentinisation, harzburgite HSE compositions are mostly (6 out of 8 samples) indistinguishable from abyssal peridotites, and only slightly more radiogenic in their Os isotopic composition. Two lines of evidence suggest that SSZ melt percolation occurred through mantle that was compositionally heterogeneous at ~492 Ma. The first is that two (dunitised) harzburgites yield model ages of 1.1–1.2 Ga, suggesting that melt infiltration has in some way been responsible for revealing these ages. The other line of evidence is that a suite of thin (mm–cm) dunite channels have radiogenic initial Os isotope compositions as a consequence of containing high Re/Os sulphides. The high Re/Os component has presumably been remobilised from the host harzburgite. The thin dunite sheets also have enhanced Pt and Pd concentrations. By contrast, a much thicker (~5 m) dunite sheet has a relatively low initial Os isotope composition and depleted Pd and Re concentrations. The differences in the HSE and Os isotope characteristics of the various dunites reflect both the heterogeneities present in the harzburgitic mantle wedge through which the SSZ melt percolated, the long-lived nature of some upper mantle melt channels compared to others and/or changes in the composition of the melts over the lifetime of the subduction zone. The Viels peridotites provide new constraints on the length-scales and physical nature of mantle Os isotopic heterogeneities, and support the notion that refractory domains can be controlled at the grain-scale in the oceanic mantle.

Acknowledgements

B.O'D. acknowledges support from a Royal Society Research Grant (RG100528) and from Natural Environment Research Council (NERC) New Investigator grant NE/J00457X/1 and Standard Grant NE/L004011/1. NSF grants (EAR-1423879 and EAR-1447130) to RJW and JMDD, respectively, are gratefully acknowledged. J.S.D. gratefully acknowledges a UCD Seed Funding Grant and Science Foundation Ireland Grant No. 13/RC/2092, which is co-funded under the European Regional Development Fund. Michael Bizimis and an anonymous reviewer are thanked for their constructive reviews.

Appendix A. Supplementary material

Supplementary material related to this article can be found online at https://doi.org/10.1016/j.epsl.2018.02.020.

References

Alard, O., Luguet, A., Pearson, N.J., Griffin, W.L., Lorand, J.-P., Gannoun, A., Burton, K.W., O'Reilly, S.Y., 2005. In situ Os isotopes in abyssal peridotites bridge the isotopic gap between MORBs and their source mantle. Nature 436, 1005–1008.

Anbar, A.D., Creaser, R.A., Papanastassiou, D.A., Wasserburg, G.J., 1992. Rhenium in seawater: confirmation of generally conservative behaviour. Geochim. Cosmochim. Acta 56, 4099–4103.

Arai, S., Yurimoto, H., 1994. Podiform chromitites of the Tari–Misaka Ultramafic Complex, southwestern Japan, as mantle–melt interaction products. Econ. Geol. 89, 1279–1288.

Becker, H., Dale, C.W., 2016. Re–Pt–Os isotopic and highly siderophile element behavior in oceanic and continental mantle tectonite. Rev. Mineral. Geochem. 81, 369–440.

Becker, H., Horan, M.F., Walker, R.J., Gao, S., Lorand, J.-P., Rudnick, R.L., 2006. Highly siderophile element composition of the Earth's primitive upper mantle: constraints from new data on peridotite massifs and xenoliths. Geochim. Cosmochim. Acta 70, 4528–4550.

Birck, J.L., Roy-Barman, M., Capmas, F., 1997. Re–Os isotopic measurements at the femtomole level in natural samples. Geostand. Newsl. 21, 19–27.

Bizimis, M., Griselin, M., Lassiter, J.C., Salters, V.J.M., Sen, G., 2007. Ancient recycled mantle lithosphere in the Hawaiian plume: Osmium–Hafnium isotopic evidence from peridotite mantle xenoliths. Earth Planet. Sci. Lett. 257, 259–273.

Bodinier, J.-L., Godard, M., 2003. Orogenic, ophiolitic and abyssal peridotites. In: Carlson, R.W., Holland, Heinrich D., Turekian, Karl K. (Eds.), Treatise on Geochemistry, vol. 2. Elsevier, pp. 103–170, p. 568.

Boyd, F.R., Mertzman, S.A., 1987. Composition and structure of the Kaapvaal lithosphere, southern Africa. In: Mysen, B.O. (Ed.), Magmatic Processes: Physicochemical Principles. In: Geochemical Society Special Publications, vol. 1, pp. 13–24.

Büchl, A., Brügmann, G.E., Batanova, V.G., Münker, C., Hofmann, A.W., 2002. Melt-percolation monitored by Os-isotopes and HSE abundances: a case study from the mantle section of the Troodos Ophiolite. Earth Planet. Sci. Lett. 204, 385–402.

Büchl, A., Brügmann, G.E., Batanova, V.G., Hofmann, A.W., 2004. Os mobilization during melt percolation: the evolution of Os isotope heterogeneities in the mantle sequence of the Troodos ophiolite, Cyprus. Geochim. Cosmochim. Acta 68, 3397–3408.

Burton, K.W., Cenki-Tok, B., Mokadem, F., Harvey, J., Gannoun, A., Alard, O., Parkinson, I.J., 2012. Unradiogenic lead in Earth's upper mantle. Nat. Geosci. 5 (8), 570–573.

Chew, D.M., Daly, J.S., Magna, T., Pagé, L.M., Kirkland, C.L., Whitehouse, M.J., Lam, R., 2010. Timing of ophiolite obduction in the Grampian orogen. Geol. Soc. Am. Bull. 122, 1787–1799.

Cohen, A.S., Waters, G.G., 1996. Separation of osmium from geological materials by solvent extraction for analysis by thermal ionization mass spectrometry. Anal. Chim. Acta 332, 269–275.

Crowley, Q.G., Strachan, R.A., 2015. U–Pb constraints on obduction initiation of the Unst Ophiolite: an oceanic core complex in the Scottish Caledonides? J. Geol. Soc. Lond. 172, 279–282.

Day, J.M.D., Waters, C.L., Schaefer, B.F., Walker, R.J., Turner, S., 2016. Use of hydrofluoric acid desilicification in the determination of highly siderophile element abundances and Re–Pt–Os isotope systematics in mafic-ultramafic rocks. Geostand. Geoanal. Res. 40, 49–65.

Day, J.M.D., Walker, R.J., Warren, J.M., 2017a. ^{186}Os–^{187}Os and highly siderophile element abundance systematics of the mantle revealed by abyssal peridotites and Os-rich alloys. Geochim. Cosmochim. Acta 200, 232–254.

Day, J.M.D., O'Driscoll, B., Strachan, R.A., Daly, J.S., Walker, R.J., 2017b. Identification of mantle peridotite as a possible Iapetan ophiolite sliver in south Shetland, Scottish Caledonides? J. Geol. Soc. Lond. 174, 88–92.

Derbyshire, E.J., O'Driscoll, B., Lenaz, D., Gertisser, R., Kronz, A., 2013. Compositionally heterogeneous podiform chromitite in the Shetland Ophiolite Complex (Scotland): implications for chromitite petrogenesis and late-stage alteration in the upper mantle portion of a supra-subduction zone ophiolite. Lithos 162–163, 279–300.

Dick, H.J.B., Fisher, R.L., Bryan, W.B., 1984. Mineralogic variability of the uppermost mantle along mid-ocean ridges. Earth Planet. Sci. Lett. 69, 88–106.

Dilek, Y., Furnes, H., 2011. Ophiolite genesis and global tectonics: geochemical and tectonic fingerprinting of ancient oceanic lithosphere. Geol. Soc. Am. Bull. 123, 387–411.

Flinn, D., 2001. The basic rocks of the Shetland Ophiolite Complex and their bearing on its genesis. Scott. J. Geol. 37, 79–96.

González-Jiménez, J.M., Griffin, W.L., Proenza, J.A., Gervilla, F., O'Reilly, S.Y., Akbulut, M., Pearson, N.J., Arai, S., 2014. Chromitites in ophiolites: how, where, when, why? Part II. The crystallization of chromitites. Lithos 189, 140–158.

Harvey, J., Gannoun, A., Burton, K.W., Rogers, N.W., Alard, O., Parkinson, I.J., 2006. Ancient melt extraction from the oceanic upper mantle revealed by Re–Os isotopes in abyssal peridotites from the mid-Atlantic ridge. Earth Planet. Sci. Lett. 244, 606–621.

Harvey, J., Dale, C.W., Gannoun, A., Burton, K.W., 2011. Osmium mass balance in peridotite and the effects of mantle derived sulphides on basalt petrogenesis. Geochim. Cosmochim. Acta 75, 5574–5596.

Johnson, K.T.M., Dick, H.J.B., 1992. Open system melting and temporal and spatial variation of peridotite and basalt at the Atlantis II fracture zone. J. Geophys. Res. 97, 9219–9241.

Kelemen, P.B., 1990. Reaction between ultramafic wall rock and fractionating basaltic magma: Part I. Phase relations, the origin of calc-alkaline magma series, and the formation of discordant dunite. J. Petrol. 31, 51–98.

Kelemen, P.B., Dick, H.J.B., Quick, J.E., 1992. Formation of harzburgite by pervasive melt/rock reaction in the upper mantle. Nature 358, 635–641.

Lassiter, J.C., Byerly, B.L., Snow, J.E., Hellebrand, E., 2014. Constraints from Os-isotope variations on the origin of Lena Trough abyssal peridotites and implications for the composition and evolution of the depleted upper mantle. Earth Planet. Sci. Lett. 403, 178–187.

Liu, C.-Z., Snow, J.E., Brugmann, G., Hellebrand, E., Hofmann, A.W., 2009. Non-chondritic HSE budget in Earth's upper mantle evidenced by abyssal peridotites from Gakkel ridge (Arctic Ocean). Earth Planet. Sci. Lett. 283, 122–132.

Lorand, J.-P., Alard, O., Luguet, A., 2010. Platinum-group element micronuggets and refertilization process in Lherz orogenic peridotite (northeastern Pyrenees, France). Earth Planet. Sci. Lett. 289, 298–310.

Lorand, J.-P., Luguet, A., 2016. Chalcophile and siderophile elements in mantle rocks: trace elements controlled by trace minerals. Rev. Mineral. Geochem. 81, 441–488.

Luguet, A., Shirey, S.B., Lorand, J.-P., Horan, M.F., Carlson, R.W., 2007. Residual platinum-group minerals from highly depleted harzburgites of the Lherz massif (France) and their role in HSE fractionation of the mantle. Geochim. Cosmochim. Acta 71, 3082–3097.

Mallick, S., Standish, J.J., Bizimis, M., 2015. Constraints on the mantle mineralogy of an ultra-slow ridge: hafnium isotopes in abyssal peridotites and basalts from the 9–25 E Southwest Indian Ridge. Earth Planet. Sci. Lett. 410, 42–53.

McDonough, W.F., Sun, S-s., 1995. The composition of the Earth. Chem. Geol. 120, 223–253.

Morgan, J.W., 1986. Ultramafic xenoliths: clues to Earth's late accretionary history. J. Geophys. Res., Solid Earth 91 (B12), 12375–12387.

Morgan, J.W., Walker, R.J., Brandon, A.D., Horan, M.F., 2001. Siderophile elements in Earth's upper mantle and lunar breccias: data synthesis suggests manifestations of the same late influx. Meteorit. Planet. Sci. 36, 1257–1275.

Mukhopadhyay, S., 2012. Early differentiation and volatile accretion recorded in deep-mantle neon and xenon. Nature 486 (7401), 101–104.

Mundl, A., Touboul, M., Jackson, M.G., Day, J.M.D., Kurz, M.D., Lekic, V., Helz, R.T., Walker, R.J., 2017. Tungsten-182 heterogeneity in modern ocean island basalts. Science 356, 66–69.

O'Driscoll, B., Day, J.M.D., Walker, R.J., Daly, J.S., McDonough, W.F., Piccoli, P.M., 2012. Chemical heterogeneity in the upper mantle recorded by peridotites and chromitites from the Shetland Ophiolite Complex, Scotland. Earth Planet. Sci. Lett. 333–334, 226–237.

O'Driscoll, B., González-Jiménez, J.M., 2016. Petrogenesis of the platinum-group minerals. Rev. Mineral. Geochem. 81, 489–578.

O'Driscoll, B., Walker, R.J., Day, J.M.D., Ash, R.D., Daly, J.S., 2015. Generations of melt extraction, melt–rock interaction and high-temperature metasomatism preserved in peridotites of the ~497 Ma Leka Ophiolite Complex, Norway. J. Petrol. 56, 1797–1828.

Parkinson, I.J., Pearce, J.A., 1998. Peridotites from the Izu–Bonin–Mariana Forearc (ODP Leg 125): evidence for mantle melting and melt–mantle interaction in a supra-subduction zone setting. J. Petrol. 39, 1577–1618.

Pearce, J.A., Parkinson, I.J., 1993. Trace element models for mantle melting: application to volcanic arc petrogenesis. In: Prichard, H.M., Alabaster, T., Harris, N.B.W., Neary, C.R. (Eds.), Magmatic Processes and Plate Tectonics. In: Special Publications, vol. 76. Geological Society, London, pp. 373–403.

Pearson, D.G., Parman, S.W., Nowell, G.M., 2007. A link between large mantle melting events and continent growth seen in osmium isotopes. Nature 449, 202–205.

Prichard, H.M., Barnes, S.J., Dale, C.W., Godel, B., Fisher, P.C., Nowell, G.M., 2017. Paragenesis of multiple platinum-group mineral populations in Shetland ophiolite chromitite: 3D X-ray tomography and in situ Os isotopes. Geochim. Cosmochim. Acta 216, 314–334.

Rampone, E., Hofmann, A.W., 2012. A global overview of isotopic heterogeneities in the oceanic mantle. Lithos 148, 247–261.

Schulte, R.F., Schilling, M., Horan, M.F., Anma, R., Komiya, T., Farquhar, J., Piccoli, P.M., Pitcher, L., Walker, R.J., 2009. Chemical and chronologic complexity in the convecting upper mantle: evidence from the Taitao Ophiolite, southern Chile. Geochim. Cosmochim. Acta 73, 5793–5819.

Shi, R., Alard, O., Zhi, X., O'Reilly, S.Y., Pearson, N.J., Griffin, W.L., Zhang, M., Chen, X., 2007. Multiple events in the Neo-Tethyan oceanic upper mantle: evidence from Ru–Os–Ir alloys in the Luobusa and Dongqiao ophiolitic podiform chromitites, Tibet. Earth Planet. Sci. Lett. 261 (1–2), 33–48.

Shirey, S.B., Walker, R.J., 1998. The Re–Os isotope system in cosmochemistry and high-temperature geochemistry. Annu. Rev. Earth Planet. Sci. 26, 423–500.

Snow, J.E., Hart, S.R., Dick, H.J.B., 1994. Nd and Sr isotopic evidence for a link between mid-ocean ridge basalts and abyssal peridotites. Nature 371, 57–60.

Snow, J.E., Reisberg, L., 1995. Os isotopic systematics of the MORB mantle: results from altered abyssal peridotites. Earth Planet. Sci. Lett. 133, 411–421.

Spray, J.G., Dunning, G.R., 1991. A U/Pb age for the Shetland Islands oceanic fragment, Scottish Caledonides: evidence from anatectic plagiogranites in 'layer 3' shear zones. Geol. Mag. 128 (6), 667–671.

Stracke, A., Snow, J.E., Hellebrand, E., von der Handt, A., Bourdon, B., Birbaum, K., Gunther, D., 2011. Abyssal peridotite Hf isotopes identify extreme mantle depletion. Earth Planet. Sci. Lett. 308, 359–368.

Walker, R.J., Brandon, A.D., Bird, J.M., Piccolli, P.M., McDonough, W.F., Ash, R.D., 2005. ^{187}Os–^{186}Os systematics of Os–Ir–Ru alloy grains from southwestern Oregon. Earth Planet. Sci. Lett. 230, 211–226.

Walker, R.J., Hanski, E.J., Vuollo, J., Liipo, J., 1996. The Os isotopic composition of Proterozoic upper mantle: evidence for chondritic upper mantle from the Outokumpu ophiolite, Finland. Earth Planet. Sci. Lett. 141, 161–173.

Warren, J.M., 2016. Global variations in abyssal peridotite compositions. Lithos 248–251, 193–219.

Warren, J.M., Shimizu, N., Sakaguchi, C., Dick, H.J.B., Nakamura, E., 2009. An assessment of mantle heterogeneity based on abyssal peridotite isotopic compositions. J. Geophys. Res. 114, B12203.

Workman, R.K., Hart, S.R., 2005. Major and trace element composition of the depleted MORB mantle (DMM). Earth Planet. Sci. Lett. 231, 53–72.